Available online at www.sciencedirect.com
ScienceDirect
JOURNAL OF IRON AND STEEL RESEARCH, INTERNATIONAL. 2015, 22(1): 55-59

Microstructure Evolution and Microhardness of Ultrafine-grained High Carbon Steel during Multiple Laser Shock Processing

Yi XIONG[1,2], Tian-tian HE[3], Feng-zhang REN[1,2], Peng-yan LI[1], Lu-fei CHEN[1], Alex A. VOLINSKY[4]

(1. School of Materials Science and Engineering, Henan University of Science and Technology, Luoyang 471003, Henan, China; 2. Henan Collaborative Innovation Center of Non-ferrous Metal Generic Technology, Luoyang 471003, Henan, China; 3. Institute of Metal Research, Chinese Academy of Sciences, Shenyang 110016, Liaoning, China; 4. Department of Mechanical Engineering, University of South Florida, Tampa FL 33620, USA)

Abstract: Surface microstructure and microhardness of (ferrite+cementite) microduplex structure of the ultrafine-grained high carbon steel after laser shock processing (LSP) with different impact times were investigated by means of scanning electron microscopy (SEM), transmission electron microscopy (TEM), X-ray diffraction (XRD) and microhardness measurements. Equiaxed ferrite grains were refined from 400 to 150 nm, and the cementite lamellae were fully spheroidized, with a decrease of the particle diameter from 150 to 100 nm as the impact times increased. The cementite dissolution was enhanced significantly. Correspondingly, the lattice parameter of α-Fe and microhardness increased with the impact times.

Key words: ultrafine-grained high carbon steel; laser shock processing; impact times; microstructure; microhardness

Laser shock processing (LSP) is a new surface modification technology for improving metal mechanical properties at ultra-high strain rates (10^6 — 10^7 s^{-1})[1]. Shock waves generated during LSP originate from the plasma volume expansion formed on the material surface when it is irradiated with a laser operated in the nanosecond or sub-nanosecond range with power density typically greater than 10^9 W/cm^2. This shock wave alters the surface microstructure and mechanical properties of materials, such as hardness and fatigue strength[2,3]. The fatigue strength increases due to the surface compressive residual stresses introduced by the shock waves[4]. The increase in hardness and yield strength is attributed to the high density arrays of dislocations in several alloys[5] and deformation twins in some ferrous alloys[6] generated by laser shock wave. Therefore, LSP has been used to harden the surface and improve the mechanical properties of some structural metal components made from magnesium alloys[7], aluminum alloys[8], copper[9] and titanium alloys[10].

Steels are widely used in the industry. LSP of steel has been extensively studied and reported in the literature. For example, Nikitin et al.[11,12] compared the near surface microstructure change and fatigue life improvement of AISI 304 stainless steel after LSP and deep rolling (DR). Hu and Yao[13] investigated LSP of AISI 1045 steel by finite element modeling, and the results were validated by experiments. Chu et al.[14] compared microstructure, hardness and residual stress generated by LSP, DR and shot peening (SP) on Hadfield manganese steel. In the study performed by Chu et al., it was found that LSP resulted in a large hardness increase due to the high density ε-martensite phase formation. Lu et al.[5,6] investigated LSP of LY2 Al alloy and AISI 304 stainless steel by single and multiple pulses. The effect of grain refinement by multiple pulse LSP was superior to that by a single pulse, revealing the underlying grain refinement mechanism. Recently, tra-

Foundation Item: Item Sponsored by National Natural Science Foundation of China (50801021, 51201061); Program for Young Key Teachers in Henan Province of China (2011GGJS-070); Program for Henan Province for Science and Technology Innovation Excellent Talents of China (144200510001)

Biography: Yi XIONG, Doctor, Associate Professor; **E-mail**: xy_hbdy@163.com; **Received Date**: March 4, 2014

ditional materials with coarse micrometer-level grains have been studied extensively. Compared with traditional materials, the ultrafine-grained materials have some special properties. However, few studies have focused on the similarities and differences of microstructure and mechanical properties between the ultrafine-grained materials and the traditional materials during LSP. In previous work[15], surface microstructure and residual stress of ultrafine-grained high carbon steel after LSP with different laser impact energies were investigated. However, the effect of the impact times on microstructure and mechanical properties of the ultrafine-grained materials is still unknown.

Therefore, the aim of this work is to investigate the effects of multiple LSP impacts on microstructure and microhardness of the ultrafine-grained materials. The underlying microstructure evolution mechanism after LSP was revealed.

1 Experimental

1.1 Experimental materials

The material used in this study was commercial T8 steel. The chemical composition of T8 steel is shown in Table 1. To ensure the full evolution of pearlite, all specimens were vacuum annealed at 1273 K for 30 min and then placed into a salt bath furnace at 873 K for 30 min, followed by water cooling outside the furnace. The samples were subsequently machined into cylindrical bars of 49 mm in length and 8.3 mm in diameter.

Table 1 Chemical composition of T8 steel mass%

C	S	Si	Mn	P	Cr	Ni	Cu	Fe
0.82	0.012	0.244	0.334	0.011	0.09	0.043	0.124	Balance

The equal channel angular pressing (ECAP) was done in the Division of Special Steels of Central Iron and Steel Research Institute, China. The ECAP experiments were conducted using a split die with two channels intersecting at an inner angle of 120° and an outer angle of 30°. Samples were subjected to four ECAP passes at 923 K using the Bc route method, in which each specimen was rotated 90° along the longitudinal axis between the passes. The samples used for LSP were cut into a circular shape with dimensions of ϕ8 mm×2 mm. Prior to the LSP treatment, sample surface was polished with different grade SiC papers (500 to 2400 grit), followed by cleaning in deionized water. Ultrasound cleaning in ethanol was used to degrease the sample surface, and LSP was conducted shortly after the sample preparation.

1.2 LSP parameters

The LSP experiments were performed using a solid state Nd:glass phosphate laser operated at 5 Hz with a wavelength of 1064 nm, and the full width at half maximum (FWHM) of the pulses was about 15 ns. The laser beam spot size on the sample was 3 mm. Samples were submerged into a water bath where they were treated with LSP. A water layer, about 1 mm thick, was used as the transparent confining layer, and commercial 100 μm thick Al tape was used as an absorbing layer to protect the sample surface from thermal effects. The samples were treated respectively by 2, 4, and 6 LSP impacts with the same laser pulse energy of 2 J. The processing parameters used in LSP are listed in Table 2. During multiple LSP impacts, the laser beam was perpendicular to the sample surface, treating the same area of the sample, and the Al tape was replaced after each of the multiple LSP impacts.

Table 2 Processing parameters used in LSP

Type	Value
Beam divergence of output/mrad	≤2
Spot diameter/mm	3
Pulse energy/J	2
Impact times	2, 4, 6
Pulse width/ns	<15
Repetition rate/Hz	5
Laser wavelength/nm	1064
Energy stability	<1.5%

1.3 Microstructure characterization

Field-emission scanning electron microscopy (FESEM, QUANTA FEG650) was used for surface morphology analysis. The specimens were etched using 4% nital solution after LSP. Transmission electron microscopy (TEM, JEM-2010) was used to examine the microstructure of the processed specimens. Thin foil, mechanically polished down to 40 μm, was utilized for TEM sample preparation by using a double jet electrolytic thinning technique (30 V, 50 mA) in a 93 vol. % acetic acid and 7 vol. % perchloric acid mixture. Liquid nitrogen was used for cooling during the thinning process, with the temperature rising not higher than 243 K.

A D8 ADVANCE X-ray diffractometer (XRD) with CuKα radiation was used to determine the phase changes. The tube voltage and current were 35 kV and

40 mA, respectively. The tube anode was CuKα1 (λ = 0.15406 nm), and the width of the receiving silt was 2 mm. The final lattice parameter of ferrite was calculated from the obtained data by means of extrapolation and the least square method.

1.4 Measurements of microhardness

Microhardness of the laser processed regions was measured by using an MH-3 Vickers microhardness tester with normal load of 2 N and holding time of 10 s on the as-polished and laser processed regions. An average microhardness value was determined based on 5 indentation measurements.

2 Results and Discussion

2.1 Microstructure evolution

Microstructure of the ultrafine-grained steel before and after LSP is shown in Fig. 1. Figs. 1(a) and 1(b) show the SEM and TEM micrographs of the samples before LSP. After four ECAP passes, the microstructure changes from lamellar pearlite to an ultrafine (ferrite + cementite) microduplex structure. The average grain size of ferrite is 400 nm and the particle diameter of the cementite is about 150 nm. In some regions, the short bar shaped cementite can still be observed. The microstructure and mechanical

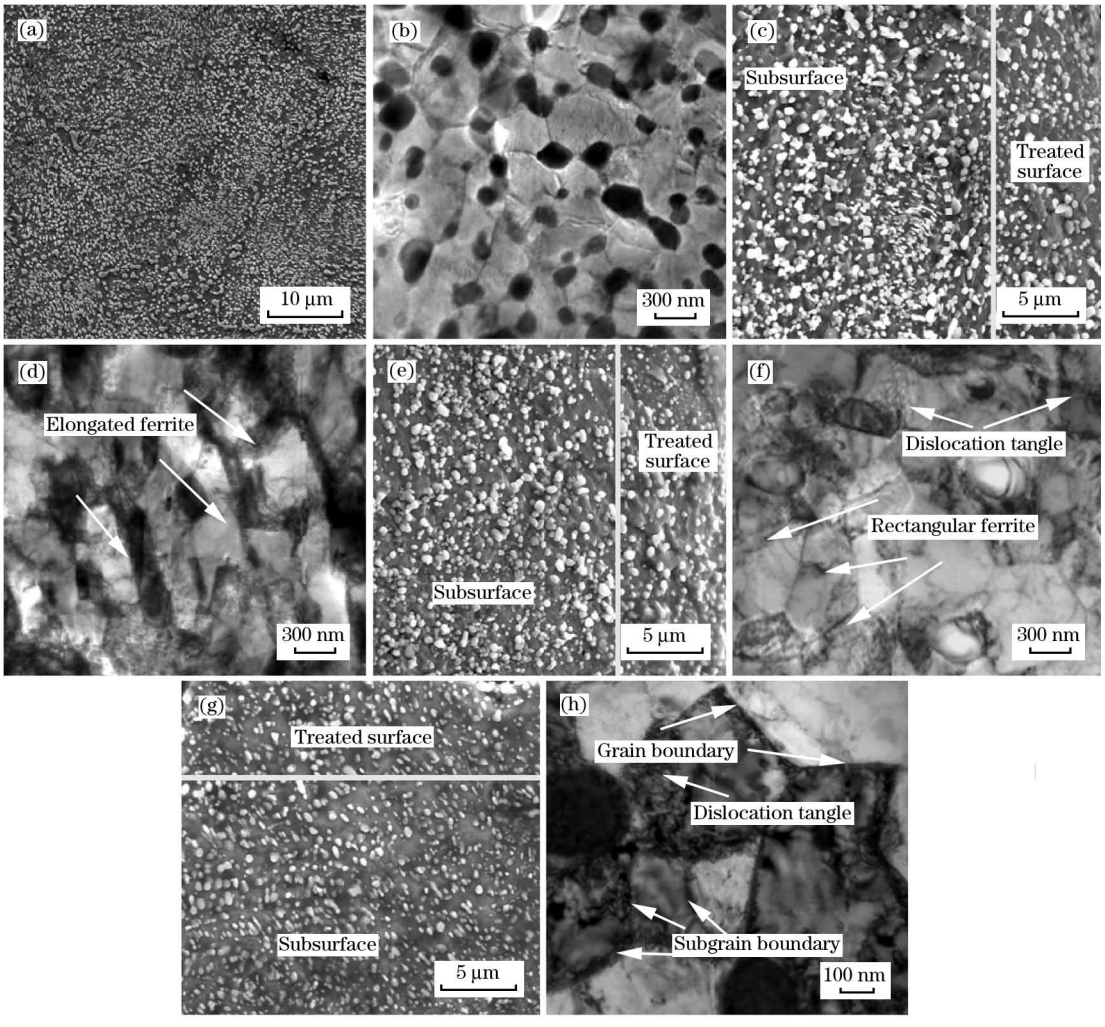

(a) SEM, before LSP; (b) TEM, before LSP; (c) SEM, after 2 LSP impacts; (d) TEM, after 2 LSP impacts; (e) SEM, after 4 LSP impacts; (f) TEM, after 4 LSP impacts; (g) SEM, after 6 LSP impacts; (h) TEM, after 6 LSP impacts.

Fig. 1 SEM and TEM micrographs of ultrafine-grained steel microstructure before and after LSP

properties of ECAPed ultrafine-grained high carbon steel were investigated in the previous work[16,17].

After 2 LSP impacts, some short bar shaped cementite is still present (the ellipse in Fig. 1(c)). The amount of the cementite particles on the surface is less than that in the subsurface, and the corresponding particle diameter of the surface is slightly larger than that of the subsurface, as seen in Fig. 1

(c). Meanwhile, dislocations were generated and accumulated in the ferrite due to the severe plastic deformation, and the shape of the ferrite was changed from equiaxed to elongated grains, as seen in Fig. 1 (d). After 4 LSP impacts, the short bar shaped cementite disappeared completely. The cementite particle size is inhomogeneously distributed. As seen in Fig. 1(e), the size of the large particles is 300 nm, while the size of the small ones is about 50 nm. The shape of the ferrite is changed from elongated to rectangular grains, and the average grain size of ferrite is around 300 nm. With more LSP impacts, a large amount of high density tangled dislocations were observed in Fig. 1(f). After 6 LSP impacts, as seen in Figs. 1(g) and 1(h), the size of the spheroidized cementite particles is about 100 nm. Meanwhile, finer equiaxed ferrite grains were formed, with an average grain size of 150 nm. This is mainly due to more dislocations formed after each LSP impact. Dislocation lines pile-up contributes to the formation of dislocation tangles and dense dislocation walls (Fig. 1(h)). During multiple LSP impacts, the second LSP impact may lead to the change of slip systems along the depth direction, even inside the same grain, so dislocation tangles and dense dislocation walls could lead to subgrain boundaries separating individual cells. Finally, subgrains with a width of 100 nm form, which eventually transform into equiaxed refined grains by the development of subgrain boundaries, as seen from Fig. 1(h). The evolution of the continuously dynamic recovery and recrystallization in subgrain boundaries leads to a gradual transition of boundaries character until the formation of refined grain boundaries[18]. After multiple LSP impacts, the strain and strain rate increase further, and dislocation tangles and dense dislocation walls could form inside the refined grains, indicating that the refined grains could be subdivided following a similar mechanism. As a result, the ultrafine-grained structures were further refined. Similar phenomenon was also observed in AISI 8620 steel by multiple LSP impacts[19].

2.2 XRD analysis

Fig. 2 shows the XRD patterns of the ultrafine-grained steel before and after LSP. Compared with the ultrafine-grained steel after 4 passes of ECAP, the α-Fe peaks of the samples after LSP shift to smaller diffraction angles. More LSP impacts significantly shift the α-Fe peaks towards the smaller diffraction angles. The lattice parameter of α-Fe is 0.28578 nm in the ultrafine-grained steel. With more LSP impacts, the lattice parameter of α-Fe increased. After LSP with 2, 4 and 6 impacts, the lattice parameter of α-Fe is 0.28613, 0.28631 and 0.28653 nm, respectively. The carbon content in the pearlite ferrite after different impact times can be estimated according to the relationship between the lattice parameter and carbon content of α-Fe given by Fasiska and Wagenblas[20]. Corresponding change of the carbon content in α-Fe is 0.09%, 0.14% and 0.19% after 2, 4 and 6 impacts, respectively. This indicates that the cementite dissolution results in the increase of the carbon content, leading to the increase of α-Fe lattice parameters. Similar changes of α-Fe lattice parameters were reported in previous study for cold-rolled pearlitic steels[21]. LSP is a cold processing technique[22,23]. During ultra-high strain rates deformation introduced by shock wave, the cementite is in the form of bent, kink, fracture, and even dissolution to coordinate the deformation of the ferrite. More LSP impacts lead to higher cementite dissolution and a more significant left shift of the α-Fe peaks.

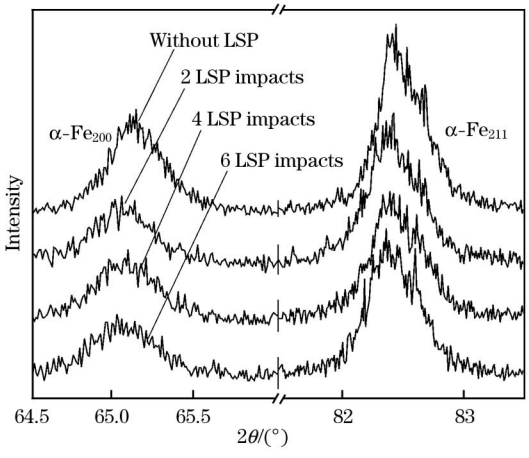

Fig. 2 Changes of XRD peak position of α-Fe in ultrafine-grained structure before and after different number of LSP impacts

2.3 Microhardness analysis

Measured microhardness values of the ultrafine-grained steel near the surface after different LSP impact times are shown in Fig. 3. Microhardness increases with LSP impact times. Meanwhile, microhardness in the impact center is obviously higher compared with the corresponding values at the edge. This is because the stress induced by the shock wave has a Gaussian distribution due to the character of the laser pulse energy[22]. In the impact center, severe plastic deformation occurred, so the microhard-

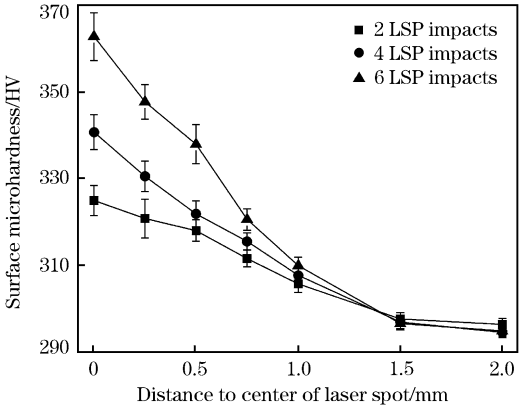

Fig. 3 Microhardness of ultrafine-grained structure after different LSP impacts

ness is higher than that in other regions. With more LSP impacts, the depth of severe plastic deformation increased. After 2, 4 and 6 LSP impacts, the microhardness in the impact center increased by 11.7%, 17.2%, and 24.7% from 291 HV (before LSP) to 325, 341 and 363 HV, respectively. It can be seen that the microhardness is increased by 4.9% and 6.5% when the impact times increased from 2 to 4 and from 4 to 6, respectively. This indicates that the microhardness in the impact center tends to rise with more LSP impacts. With more LSP impacts, the grain is further refined and the dislocation density in the ferrite increases significantly. Due to the joint action of the dislocation strengthening and grain refinement, the microhardness in the impact center increases with LSP impact times.

3 Conclusions

(1) With more LSP impacts, the ultrafine-grained high carbon steel was further refined. The shape of ferrite grains changes significantly from equiaxed structures (before LSP) to elongated grains (2 LSP impacts), then to rectangular shapes (4 LSP impacts), and then to finer equiaxed structures (6 LSP impacts). The grain size of ferrite is refined from 400 nm (before LSP) to 150 nm (6 LSP impacts). The cementite lamellae are fully spheroidized and the particle diameter of the cementite is decreased from 150 nm (before LSP) to 100 nm (6 LSP impacts).

(2) The lattice parameter of α-Fe increases from 0.28578 nm prior to LSP to 0.28653 nm after 6 LSP impacts, indicating that the cementite dissolution increases with more LSP impacts. The corresponding change of the carbon content in α-Fe increases to 0.19% after 6 LSP impacts.

(3) The value of the microhardness increases with the increase of LSP impact times. After 6 LSP impacts, the microhardness increases from 291 HV (before LSP) to 363 HV.

References:

[1] C. S. Montross, T. Wei, L. Ye, G. Clark, Y. W. Mai, Int. J. Fatigue 24 (2002) 1021-1036.
[2] C. Ye, S. Suslov, B. J. Kim, E. A. Stach, G. J. Cheng, Acta Mater. 59 (2011) 1014-1025.
[3] R. Melookaran, A. Melaibari, C. Deng, P. Molian, Mater. Des. 35 (2012) 235-242.
[4] Y. X. Hu, Z. Q. Yao, F. Wang, J. Hu, Surf. Eng. 13 (2007) 470-478.
[5] J. Z. Lu, K. Y. Luo, Y. K. Zhang, C. Y. Cui, G. F. Sun, J. Z. Zhou, L. Zhang, J. You, K. M. Chen, J. W. Zhong, Acta Mater. 58 (2010) 3984-3994.
[6] J. Z. Lu, K. Y. Luo, Y. K. Zhang, G. F. Sun, Y. Y. Gu, J. Z. Zhou, X. D. Ren, X. C. Zhang, L. F. Zhang, K. M. Chen, C. Y. Cui, Y. F. Jiang, A. X. Feng, L. Zhang, Acta Mater. 58 (2010) 5354-5362.
[7] Y. K. Zhang, J. You, J. Z. Lu, C. Y. Cui, Y. F. Jiang, X. D. Ren, Surf. Coat. Technol. 204 (2010) 3947-3953.
[8] B. Rouleau, P. Peyre, J. Breuils, H. Pelletier, T. Baudin, F. Brisset, Surf. Sci. 257 (2011) 7195-7203.
[9] M. A. Meyers, F. Gregori, B. K. Kad, M. S. Schneider, D. H. Kalantar, B. A. Remington, G. Ravichandran, T. Boehly, J. S. Wark, Acta Mater. 51 (2003) 1211-1228.
[10] Z. Zhou, S. Bhamare, G. Ramakrishnan, S. R. Mannava, K. Langer, Y. H. Wen, D. Qian, V. K. Vasudevan, Surf. Coat. Technol. 206 (2012) 4619-4627.
[11] I. Nikitin, B. Sholtes, H. J. Maier, I. Altenberger, Scripta Mater. 50 (2004) 1345-1350.
[12] I. Nikitin, I. Altenberger, Mater. Sci. Eng. A 465 (2007) 176-182.
[13] Y. X. Hu, Z. Q. Yao, Surf. Coat. Technol. 202 (2008) 1517-1525.
[14] J. P. Chu, J. M. Rigsbee, G. Banás, F. V. Lawrence, H. E. Elsayed-ali, Metall. Mater. Trans. A 26 (1995) 1507-1517.
[15] Y. Xiong, T. T. He, Z. Q. Guo, H. Y. He, F. Z. Ren, A. A. Volinsky, Mater. Sci. Eng. A 570 (2013) 82-86.
[16] Y. Xiong, T. T. He, Z. Q. Guo, H. Y. He, F. Z. Ren, A. A. Volinsky, Mater. Sci. Eng. A 563 (2013) 163-167.
[17] T. T. He, Y. Xiong, F. Z. Ren, Z. Q. Guo, A. A. Volinsky, Mater. Sci. Eng. A 535 (2012) 306-310.
[18] A. Belyakov, T. Sakai, H. Miura, R. Kaibyshev, K. Tsuzaki, Acta Mater. 50 (2002) 1547-1557.
[19] J. Z. Lu, J. W. Zhong, K. Y. Luo, L. Zhang, F. Z. Dai, K. M. Chen, Q. W. Wang, J. S. Zhong, Y. K. Zhang, Mater. Sci. Eng. A 528 (2011) 6128-6133.
[20] E. J. Fasiska, H. Wagenblas, Soc. AIME. 239 (1967) 1818-1820.
[21] W. T. Fu, Y. Xiong, J. Zhao, Y. Li, T. Furuhara, T. Maki, J. Mater. Sci. Technol. 21 (2005) 25-27.
[22] X. Scherpereel, P. Peyre, R. Fabbro, R. Fabbro, G. Lederer, N. Celatil, Proc. SPIE-Int. Soc. Opt. Eng. 3097 (1997) 546-557.
[23] L. Chen, H. Zhou, Z. H. Zhang, L. Q. Ren, J. Iron Steel Res. Int. 16 (2009) No. 4, 39-43.